Chinese Chemical Letters 32 (2021) 3169–3174

Contents lists available at ScienceDirect

Chinese Chemical Letters

journal homepage: www.elsevier.com/locate/cclet

Communication

Preparation of silicon-doped ferrihydrite for adsorption of lead and cadmium: Property and mechanism

Yiran Song, Zhuanjun Zhao*, Jing Li, Yang You, Xiangbang Ma, Jie Li, Xiuwen Cheng*

Key Laboratory of Western China's Environmental Systems (Ministry of Education) and Key Laboratory for Environmental Pollution Prediction and Control, College of Earth and Environmental Sciences, Lanzhou University, Lanzhou 730000, China

ARTICLE INFO

Article history:
Received 14 December 2020
Received in revised form 17 January 2021
Accepted 1 March 2021
Available online 3 March 2021

Keywords:
Silicon-doped ferrihydrite
Water treatment
Lead
Cadmium
Adsorption mechanism

ABSTRACT

In this study, Si-doped ferrihydrite (Si-Fh) was successfully synthesized by a simple coprecipitation method for removal of heavy metals in water. Subsequently, the physicochemical properties of Si-Fh before and after adsorption were further studied using several techniques. The Si-Fh exhibited good adsorption capacity for heavy metal ions such as Pb(II) and Cd(II). The maximum adsorption capacities of lead and cadmium are respectively 105.807, 37.986 mg/g. The distribution coefficients of the materials for Pb(II) and Cd(II) also showed a great affinity (under optimal conditions). Moreover, it was found that the adsorption fit well with the Freundlich isotherm and pseudo-second-order kinetic model which means this was a chemical adsorption process. It can be conducted from both characterization and model results that adsorption of Pb(II) and Cd(II) was mainly through the complexation interaction of abundance oxygen functional groups on the surface of Si-Fh. Overall, the Si-Fh adsorbents with many superiorities have potential for future applications in the removal of Pb(II) and Cd(II) from wastewater.
© 2021 Chinese Chemical Society and Institute of Materia Medica, Chinese Academy of Medical Sciences. Published by Elsevier B.V. All rights reserved.

Heavy metals can accumulate in organisms due to their stability and difficulty in biodegradation, thus causing toxicity to organisms and ultimately humans [1]. Compared with the other physical and chemical treatment technologies, adsorption is a good method for the treatment of heavy metal wastewater with its stability, high efficiency, low cost and environmental protection [2]. Therefore, searching for high efficiency and low cost materials has become the main focus of heavy metal adsorption.

In recent decades, iron (hydr)oxides are often found as an important component in the remediation of pollution by affect the speciation and distribution of contaminants. Among typical iron (hydr)oxides, the ferrihydrite (Fh), an amorphous and poorly crystalline iron hydroxide, is one of the most significant natural sorbents due to its nanocrystal and nanopores resulting in a high surface area (> 200 m^2/g) and abundant reactive binding sites [3]. Therefore, Fh can adsorb typical heavy metals such as Pb(II) and Cd (II) by adsorption, coprecipitation or forming complexes, and synthetic Fh is used to treat wastewater [4]. Usually Fh is the first appeared sediment in the process of Fe^{3+} hydrolysis [5]. Pure Fh is thermodynamically unstable and is easily converted to more stable goethite or hematite with less strong adsorption ability. The rate of transformation depends on environmental conditions and the presence of coexisting ions.

Several publications indicated that incorporation of silicate into the Fh structure could cause a significant effect on the structural disorder and physicochemical properties. These studies also revealed that the presence of silicates could stabilize the structure and delay the transformation of Fh to more crystalline and stable oxides such as goethite or hematite [6]. It is reported that the transformation temperature for Fh to hematite gets higher (from 340 °C to 740 °C) with the addition of Si and the transformation time from Fh to goethite increases from less than 1 day to 1–2 weeks [7]. Furthermore, Silicates impact Fh magnetic properties, surface reactivity and adsorption properties. The point of zero charge of Fh is about 8 but decreased to 4 when the Si/Fe ratio reaches 0.35 [8]. An increase in specific surface area of Si-Fh was also observed [9]. Therefore, the addition of silicate is beneficial to improve the adsorption performance. Meanwhile, Si is the second most abundant element in the Earth's crust and the dissolved SiO_4^{2-} is plentiful in natural water. So Fh is rarely found as a chemically pure state and always contains impurities such as silicate in natural settings [6]. Although the properties of Fh with silicate have been widely reported, there are relatively few research reports on adsorption of Si-Fh, especially to heavy metals. Zhu Lijun studied the effect of silicate on the removal of hexavalent

* Corresponding authors.
E-mail addresses: zhj_zhao@lzu.edu.cn (Z. Zhao), chengxw@lzu.edu.cn (X. Cheng).

https://doi.org/10.1016/j.cclet.2021.03.001
1001-8417/© 2021 Chinese Chemical Society and Institute of Materia Medica, Chinese Academy of Medical Sciences. Published by Elsevier B.V. All rights reserved.

chromium during Fh transformation, and argued that silicate inhibited it to transform into more stable and dense iron phases [10]. It was also reported that the absorption amount of Zn(II) on the surface of Si-doped Fh samples is significantly higher than that of pure Fh, which is due to the formation of outer-sphere complexes [6].

There is a void in current knowledge as to Si-Fh adsorbed heavy metals such as Pb(II) and Cd(II). In addition, the synthetic Fh analyzed to adsorb heavy metals so far generally exhibits lower Si/Fe ratios, while data on higher Si/Fe molar ratios (such as 1) are rare. This paper examines the structure and properties of Si-Fh precipitates as well as the adsorption characteristic of Pb and Cd. The aim of this study was to research the influence of Si doped into Fh on its property adsorption performance.

In the present study, morphology and element distributions of Fh and Si-Fh before and after adsorption of Pb(II) and Cd(II) were observed by a scanning electron microscope (SEM) coupled with energy-dispersive X-ray (EDX) analyzer. The specific surface areas (SSA) and corresponding pore size were determined using nitrogen adsorption-desorption techniques. Fourier transform infrared spectroscopy (FTIR) spectra was measured in the range of 4000−400 cm^{-1} with a resolution of 2 cm^{-1}. The mineral species of Si-Fh were identified using an X-ray diffractometer. X-ray photoelectron spectroscopy (XPS) was used to investigate the surface chemical states before and after Pb(II) and Cd(II) exposure. The experimentally obtained elemental electron binding energies were referenced to the C 1s peak at 284.8 eV.

Sodium hydroxide (NaOH), cadmium nitrate tetrahydrate ($Cd(NO_3)_2{\cdot}4H_2O$), lead nitrate ($Pb(NO_3)_2$), ferric chloride hexahydrate ($FeCl_3{\cdot}6H_2O$), sodium nitrate ($NaNO_3$), sodium meta silicate nonahydrate ($Na_2SiO_3{\cdot}9H_2O$) and nitric acid (HNO_3) were all purchased from Tianjin kwangfu Fine Chemical Industry Research Institute. All the solvents were analytical grade. Meanwhile, Deionized (DI) water was used throughout this experiment. Synthesis of Si-Fh was performed by precipitation technique. Toward this end, a 0.4 mol/L iron (III) salt solution was dissolved in a beaker with continued stirring at room temperature. Meanwhile, a 0.4 mol/L sodium silicate solution was prepared from the $Na_2SiO_3{\cdot}9H_2O$ salt. Afterwards, the sodium silicate solution was added to the iron(III) salt solution. The pH of the suspension was adjusted to end point of the titration (pH 7.5 ± 0.2) by dropwise addition of NaOH. The procedure was completed no more than 30 min. Subsequently, the pH of suspension was monitored for 2 h under stirring to maintain pH 7.5. Finally, all precipitates were washed three to five times by centrifugation (2500 rpm, 10 min) and resuspension in deionized (DI) water to remove sodium and nitrate ion, freeze-dried in a vacuum freeze dryer and ground into a fine powder with a agate mortar.

Batch adsorption studies were performed to study the sorption capacity and mechanism of Pb(II) and Cd(II) on Si-Fh adsorbents in a series of adsorption experiments. Adsorption experiments were conducted in single system (only one species was present) with 50 mL polyethylene centrifuge tube as reactors. The tubes were placed on a thermostatic shaker operating at 250 rpm. All experiments were performed at 298 K for 24 h (unless otherwise specified) to reach the equilibrium. The concentration of Si-Fh was 2 g/L in all experiments. In order to investigate the influence of pH values, the initial concentrations of lead and cadmium ions were 150 mg/L and 75 mg/L, respectively. And the solution pH was adjusted to 4–9 at intervals of 1 with 0.1 mol/L HNO_3 or NaOH. In the ion strength effect experiments, a series of lead nitrate (0.16 g/L) and cadmium nitrate (0.08 g/L) solutions were prepared with different concentrations of $NaNO_3$ (from 0 to 0.2 mol/L) were prepared and adjusted to pH of 6 for $Pb(NO_3)_2$ and 8 for $Cd(NO_3)_2$. Samples were also taken at a given time interval. The different Pb(II) and Cd(II) ions initial concentrations changed from 0.05 g/L to 0.7 g/L and 0.05−0.18 g/L in the isothermal adsorption experiments. All the samples were in triplicate. After the adsorption is completed, all samples were centrifuged at 4000 rpm for five minutes and then filtered through filter paper (with a pore size of 0.01 μm). The concentration of Pb(II) and Cd(II) ions in the filtrate was measured by atomic absorption spectroscopy (AAS).

The surface morphological characteristics of Fh and Si-Fh were assessed by SEM (Fig. 1). As it is showed in Figs. 1a-d, SEM micrograph obviously revealed the morphology of Si-Fh was coarser and more irregular than Fh. Thus it was potentially

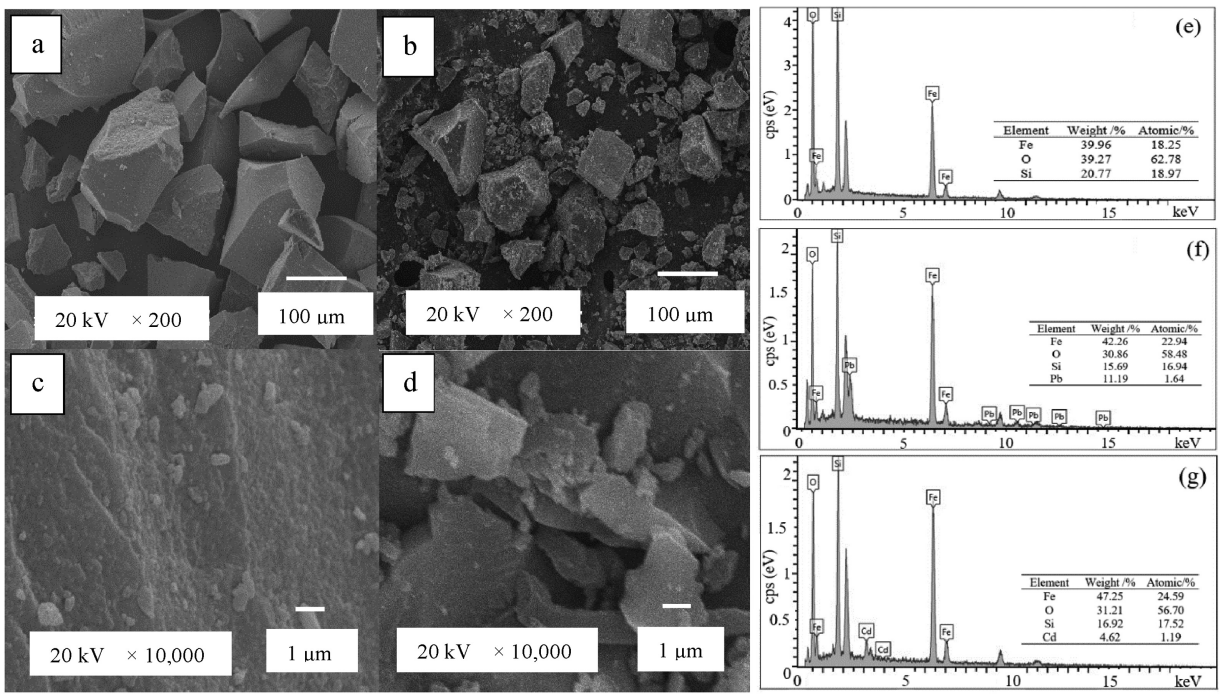

Fig. 1. SEM micrographs of Fh and Si-Fh (a-d) and EDX images of Si-Fh before (e) and after(f, g) adsorption.

beneficial to adsorption of aqueous ions [11]. The Si-Fh possessed a large amount of structural pores formed by accumulation and agglomeration. EDX analyses of Si-Fh revealed that the actual Si/Fe molar ratios are close to the original plan. Before the adsorption reaction the composition of Si-Fh was Fe (18.25%), O (62.78%), Si (18.97%), *etc.* After reaction there were decreases in the atomic percentages of both Si (16.94%) and O (58.48%) which may be due to the combination between these two elements and heavy metals. And the appearance of two new elements Pb (1.64%) and Cd (1.19%) indicated the adsorption of Pb and Cd by Si-Fh. Furthermore, the distribution of heavy metal elements was more consistent with silicon and oxygen but was different from iron which can see from the elements mapping (Fig. S1 in Supporting information). This further indicated that the adsorption of heavy metals is related to silicon and oxygen of Si-Fh.

The specific surface area of Si-Fh was 211 m^2/g according to SSA results, and the large specific surface area provided a large number of reaction sites for the direct contact of the heavy metals with the materials [12]. As shown in Fig. S2a (Supporting information), the Si-Fh had a type I isotherm with H3 hysteresis loop indicating microporous structures [13]. At low pressure ($P/P_0 < 0.02$), N_2 adsorption and desorption can also confirm the presence of micropores. This was consistent with the capillary condensation of liquid nitrogen in the mesopores formed by the aggregation of microcrystals [14]. The adsorption amount almost reached balanced when the relative pressure rose to 0.5, indicating the presence of a small amount of mesopores. There was a difference between the pore distribution of the Si-Fh before and after adsorption of Pb and Cd. The maximum value of the microporous part was 0.45 before adsorption and changed to 0.27 after adsorption. All in all, the Si-Fh was not only mainly composed of meso-pores and micro-pores but also had the large specific surface area which exposed abundant adsorption active sites and increased the adsorption properties.

FTIR was used to identify the Si-Fh functional groups before and after adsorption with Pb(II) and Cd(II) and showed that the material had rich oxygen functional groups (Fig. 2a). The FTIR spectrum consisted of the bands at 3200–3600 cm^{-1}, 1635.1, 982.8, and 678.7 cm^{-1}. The bands at 437 cm^{-1} and 982.9 cm^{-1} were related to the bending and vibrations mode of Si–O–Si respectively, which had been observed also by other investigators [15]. And a new peak at 678.7 cm^{-1} indicated the appearance of Si–O–Fe band compared with the Fh [16]. It was shown that silicates were bonded to the iron oxide phase inevitably formed Si—O—Fe bonds in other experiments [17]. Several typical bands were also observed which were a band at 1635.1 cm^{-1} and a broad band at 3200−3600 cm^{-1} assignable to O—H bending and stretching vibrations respectively [18]. Specifically, a new peak at 1384 cm^{-1} was monitored after Pb(II) and Cd(II) adsorption and attributed to the binding of O with Pb(II) and Cd(II). The XRD pattern (Fig. S3 in Supporting information) depicted two broad and weak peaks at $2\theta = 30^\circ$ and 60° which was different from the Fh. These two broad peaks both shifted to left by 4 degrees compared with the Fh. The peaks were also broader and shifted to higher d-spacings than Fh, which indicated Si incorporated into Fh [19]. Meanwhile, the particle size and crystal plane spacing d of Si-Fh increased. In this case, silicon was considered to be present in layers between crystal boundaries [20]. Moreover, there was no Na_2SiO_3 detected by XRD analyze in this experiment, which indicated there are no mineralogical changes and/or mechanistic changes of Si uptake to Fh.

XPS is a useful method to characterize the surface chemical properties of materials and the electron escape depths are 1−5 nm. The percentages indicated the area ratio of each component to the total area. And the high-resolution spectra of Fh before and after the sorption of Pb(II) and Cd(II) were reported in Figs. 2b-f and Fig. S4 (Supporting information). For Fe 2p analysis, two peaks at ~711 eV (Fe $2P_{3/2}$) and ~725 eV (Fe $2p_{1/2}$) were typically observed for the presence of Fe(III) species in ferrihydrite [21–23]. The peak at ~711 eV was due to octahedrally-coordinated lattice Fe^{3+} [24]. After Pb(II) and Cd(II) adsorption, the Fe $2p_{1/2}$ and Fe $2p_{3/2}$ peak position and intensity showed no obvious changes. Si-Fh sample exhibited three O peaks upon decomposition of the O 1s peak before adsorption in Fig. 2c. The 530.5, 531.7 and 532.8 eV peaks were assigned to O^{2-} species in ferric oxides (Fe–O–Fe), the surface Fe—O—H band and Si—O respectively [16]. The O spectra

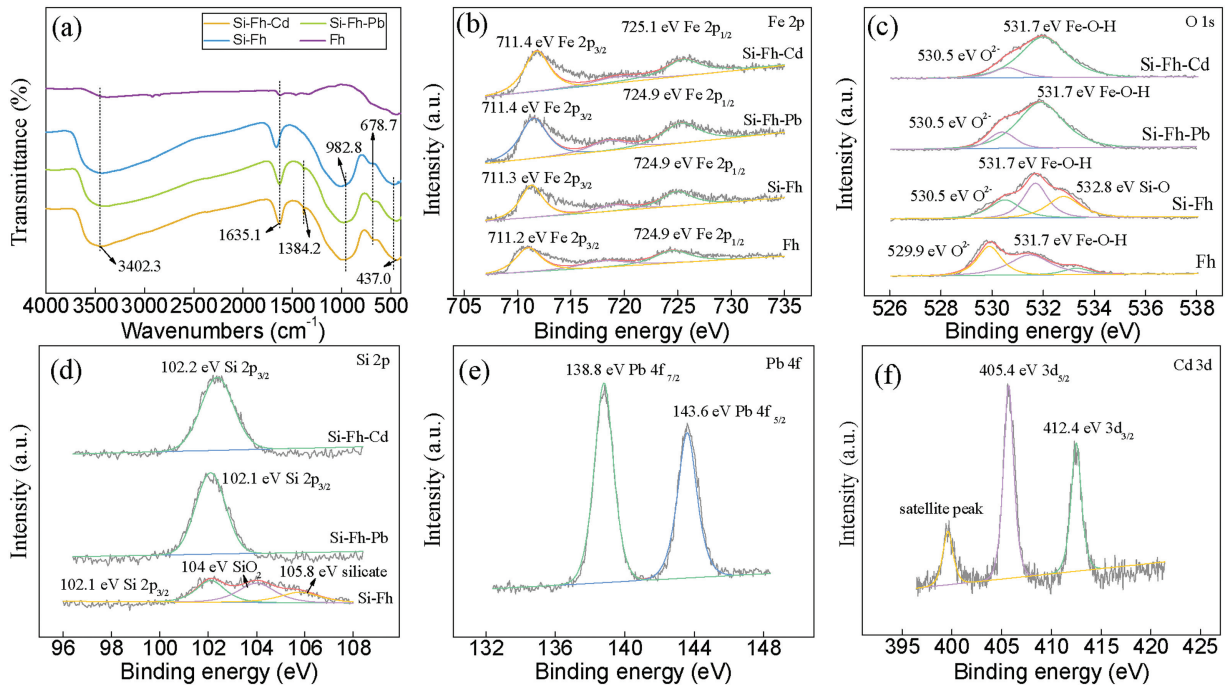

Fig. 2. (a) FTIR spectra and (b-f) XPS spectra for Fh and Si-Fh before and after reaction with Pb(II) and Cd(II).

exhibited obvious differences between the metal-loaded Si-Fh and free Si-Fh, *i.e.*, the peak at ~532.8 eV disappeared after Pb(II) or Cd(II) binding. The Fe–O–H percentage is 42.8% for materials before sorption, this component increased to 83.1% and 85.7% following Pb(II) and Cd(II) adsorption. This can be attributed to the bonding of Pb(II) and Cd(II) with Si-O fractions, resulting in the increase in Fe—O fractions in Fh samples [25]. Samples before adsorption had a broad Si peak which can be divided into three peaks 102.1, 104 and 105.8 eV. These three peaks can be assigned to Si $2p_{3/2}$, SiO_2, and silicate. In layered silicate minerals, the XPS Si peak was observed at about 102.4 eV. This similarity suggested that the silicon may be present in the tetrahedral coordination of the Fh structure [19]. The FTIR and XRD results were also consistent with the appearance of structurally incorporated silicon in the Fh sample. After adsorption, the Si peak was only at 102.1 eV and 102.2 eV for Pb or Cd in Fig. 2d. The results can also match with the O 1s spectra. The analysis of O 1s and Si 2p spectra gives spectroscopic evidences for Pb or Cd adsorption to Si-Fh mainly by Si-O complexation. XPS spectras of Pb and Cd further support the evidence on adsorption of Pb or Cd onto the surface of Si-Fh. Binding energies of Pb $4f_{7/2}$ and Pb $4f_{5/2}$ derived from spin-orbit split were 138.8 eV and 143.6 eV, respectively. Meanwhile the high-resolution XPS correlating with the binding energies of 405.4 eV and 412.4 eV were assigned to Cd $3d_{5/2}$ and Cd $3d_{3/2}$, respectively. These results further confirmed the complexation of Pb(II) and Cd(II) with oxygen functional groups of the Si-Fh during adsorption. The FTIR and XPS spectra demonstrated that the —OH groups and Si—O bands played an important role in the adsorption of Pb(II) and Cd(II).

Adsorption of heavy metals on the surface of adsorbent material is a surface reaction [26]. Therefore, pH value of aqueous solution is a variable factor that affects the species of heavy metals, the protonation of functional groups, the surface double electric layer and the adsorption process [27,28]. Fig. 3a presented the effect of initial solution pH on Pb(II) or Cd(II) sorption on Si-Fh. The removal efficiency of Pb(II) increased from 94.0%–99.8% as pH was adjusted from 4 to 6. After that, increase in pH value was accompanied with a decrease of Pb(II) adsorption amount. For Cd, the inflection point occured at pH 8, which adsorption amount reached highest. Meanwhile, the residual percentages of Cd(II) ions were higher than 5% when the pH < 6, but were decreased sharply as pH > 6. A significant factor on the heavy metals sorption process was the protonation and non-protonation of hydroxyl groups in materials. The low sorption amount of lead and cadmium by the Si-Fh in acidic environment could be interpreted to the protonation of lone pair of electrons on oxygen functional groups which means the decrease in active sites [29]. Furthermore, the surface of the materials were positively charged, which hindered the adsorption of heavy metal cations with positive charge due to the electrostatic disposal [30]. However, when the pH of solution increased, the functional groups of adsorbents surface had a tendency to deprotonate and the negative charge density increased, which were conducive to electrostatic attraction between Pb(II) or Cd(II) and Si-Fh [31]. When the pH values reached the turning point (6 for Pb and 8 for Cd), owing to the aggregation of hydroxyl ions, along with the formation of $(Pb(OH)^+$, $Cd(OH)^+)$ species, an obvious decrease in removal efficiency was observed [32]. This phenomenon can also be ascribed to the precipitation of $Pb(OH)_2$ and $Cd(OH)_2$ [33].

The mass-weighted distribution coefficient K_d (L/g) is a parameter of judging a sorbent material's affinity for some ions. The K_d values were calculated as follow (Eq. 1):

$$K_d = \frac{(C_0 - C_e)V}{C_e}m \quad (1)$$

where C_e (mg/L) is the concentration of the heavy metals at equilibrium. m (mg) is the Si-Fh mass and V (L) is the solution volume. The adsorption capacity can be considered quite good when the value of K_d > 10 L/g, and when the value >100 L/g it can be considered excellent [28,34]. In Fig. 3b, the K_d of Pb(II) and Cd(II) was higher than 100 L/g when pH = 6, 8, respectively, which indicated Si-Fh an excellent adsorbent for these metal ions. The K_d were both higher than 10 L/g when pH > 4, which suggested this material was a good adsorbent for Pb(II) and Cd(II) at most pH values.

The coexisting background ions and humic substances are common in natural and industrial water which can also affect the adsorption properties. $NaNO_3$ and humic acid (HA) were selected to research the influence of interfering substances in Figs. 3c and d. The sorption amount of Pb(II) on Si-Fh decreased slightly with the increasing of $NaNO_3$ concentration. The removal efficiency of Cd(II) showed the similar trend with Pb(II) but declined from 90.4%–42.3%, and the drop was even steeper. Similar results can be attributed to the competitive adsorption of Pb(II) or Cd(II) and coexisting ions on the surface of the material [26]. As the removal rate of cadmium decreases with the increase of ionic strength, it indicated that cadmium forms an outer-spherical complex and there were water molecules between cadmium and Si-Fh, which meant electrostatic attraction play a dominant role [31,35]. However, the removal rate of lead was not significantly affected by the ionic strength, which meant that the inner sphere complex caused by chemical bond was formed [31]. Moreover, this finding suggested that the effect of HA at 0—125 mg/L on Pb(II) or Cd(II) adsorption was not significant. This may be due to the competitive adsorption of humic acid and heavy metals on the surface of Si-Fh and the absorption of heavy metals by humic acid surface functional groups happened simultaneously, therefore the effect of the two is both not obvious.

Two main models were used to fit the adsorption kinetic. The equations are as follows,

The *pseudo*-first-order kinetic model (Eqs. 2 and 3):

$$\frac{dQ_t}{dt} = k_1(Q_e - Q_t) \quad (2)$$

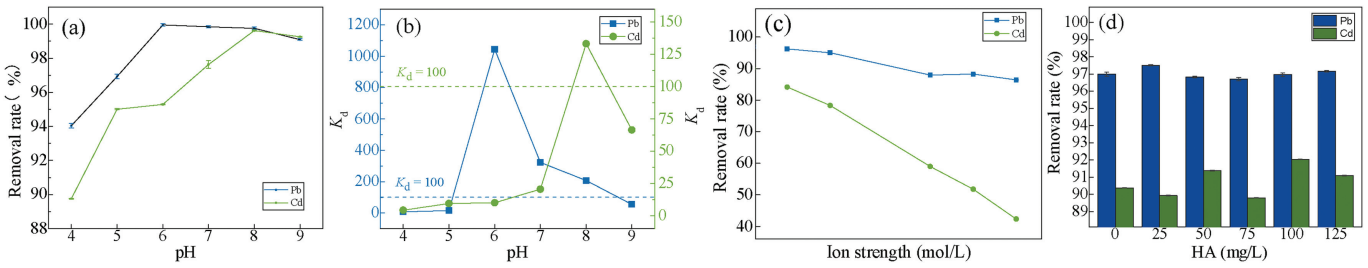

Fig. 3. (a) Effects of initial pH value on removal efficiency of Pb(II) and Cd(II) in single adsorption experiments. (b) Plots of log K_d against pH value for Pb(II) and Cd(II). Effect of ion strength (c) and humic acid (d) on the removal rate of Pb(II) and Cd(II) on the adsorbents. The error bars represent the standard deviations in triplicate (n = 3). Reaction conditions: Si-Fh concentration = 0.2 g/L, Pb concentration = 0.16 g/L, Cd concentration = 0.08 g/L, reaction temperature = 25 °C.

$$\ln(Q_e - Q_t) = \ln Q_e - k_1 t \quad (3)$$

The *pseudo*-second-order kinetic model (Eqs. 4 and 5):

$$\frac{dQ_t}{dt} = k_2(Q_e - Q_t)^2 \quad (4)$$

$$\frac{t}{Q_t} = \frac{1}{k_2 Q_e^2} + \frac{t}{Q_e} \quad (5)$$

Q_t (mg/g) and Q_e (mg/g) is the adsorption capacities at time and equilibrium, k_1 (min^{-1}) and k_2 ($g\ mg^{-1}\ min^{-1}$) are the constants of *pseudo*-first-order and *pseudo*-second-order kinetic model.

The rate controlling steps were examined by the intraparticle diffusion model and the Boyd model. These two kinetics models are given as follows:

The intraparticle diffusion model (Eq. 6):

$$Q_t = k_p t^{0.5} + C \quad (6)$$

The Boyd model (Eqs. 7 and 8):

$$B_t = -0.4944 - \ln(1-F) \quad (7)$$

$$F = Q_t/Q_e \quad (8)$$

where k_p ($mg\ g^{-1}\ min^{0.5}$) is the intraparticle diffusion effects and C is the boundary layer diffusion rate constant, respectively.

The adsorption of Pb(II) and Cd(II) were fitted by *pseudo*-first-order model and *pseudo*-second-order model. The linear forms of two kinetics models and the corresponding parameters were showed in Figs. 4a, b and Table S1 (Supporting information). The correlation coefficients (R^2) of the *pseudo*-second order model both for Pb(II) and Cd(II) were higher than those of the *pseudo*-first order model. In addition, the theoretical calculated ($Q_{e,\ cal}$) values obtained by fitting of *pseudo*-first-order kinetic model were significant different from the experimental ones ($Q_{e,\ exp}$) while the $Q_{e,\ cal}$ values of the *pseudo*-second-order model were closer to the experimental ones. These results indicated that the *pseudo*-second-order model could better fit adsorption behavior of Pb(II) and Cd(II) on Si-Fh. This meant the adsorption process was dominantly *via* a chemisorption process and both of the adsorbate and the adsorbent affected the adsorption rate by valence forces through sharing or exchange of electrons [33]. The adsorption rate and the amount of Pb was higher than that of Cd. This difference may be due to a change in the electrostatic force between Si-Fh and metal ions in the solution. The static charge force between Pb(II) and Si-Fh was stronger than Cd(II) because the static charge was inversely proportional to the ionic radius, and the hydration radius (0.401 nm) of Pb(II) was higher than Cd(II) (0.426 nm) [25]. And the electronegativity of Pb (2.10) was higher than Cd (1.69) [36].

The adsorption quantity of Pb and Cd increased rapidly in the beginning and then became slower. Finally, the adsorption equilibrium was reached. It may be related to the large number of available active sites and high affinity groups at the beginning on the surface of the Si-Fh. And then the adsorption sites on the adsorbents surface were gradually occupied. In addition, lower concentrations of heavy metals weaken the driving force to promote more collisions and contacts between heavy metal ions and the material. Under the limited bath condition, the volume concentration decreases as the solute adsorbs into the adsorbent, and typical adsorption characteristics can be described as a series of steps: (1) External diffusion, the transfer from the fluid body to the outer surface of the solid adsorbent, (2) internal diffusion, enter in the micropores of the adsorbent from the outer surface of the adsorbent and diffusion to the inner surface of the solid, (3) surface adsorption process, adsorption on the inner surface of the adsorbent solid [37,38].

Adsorption is actually a multi-step process. The rate-controlling steps can be examined using intraparticle diffusion and the Boyd models showed in Figs. 4c and d. It can be clearly observed that the plot of Q_t *versus* $t^{1/2}$ is a straight line that does not pass through the origin and the point is distributed as a scatter. This result suggested that the intraparticle diffusion was not the single process which

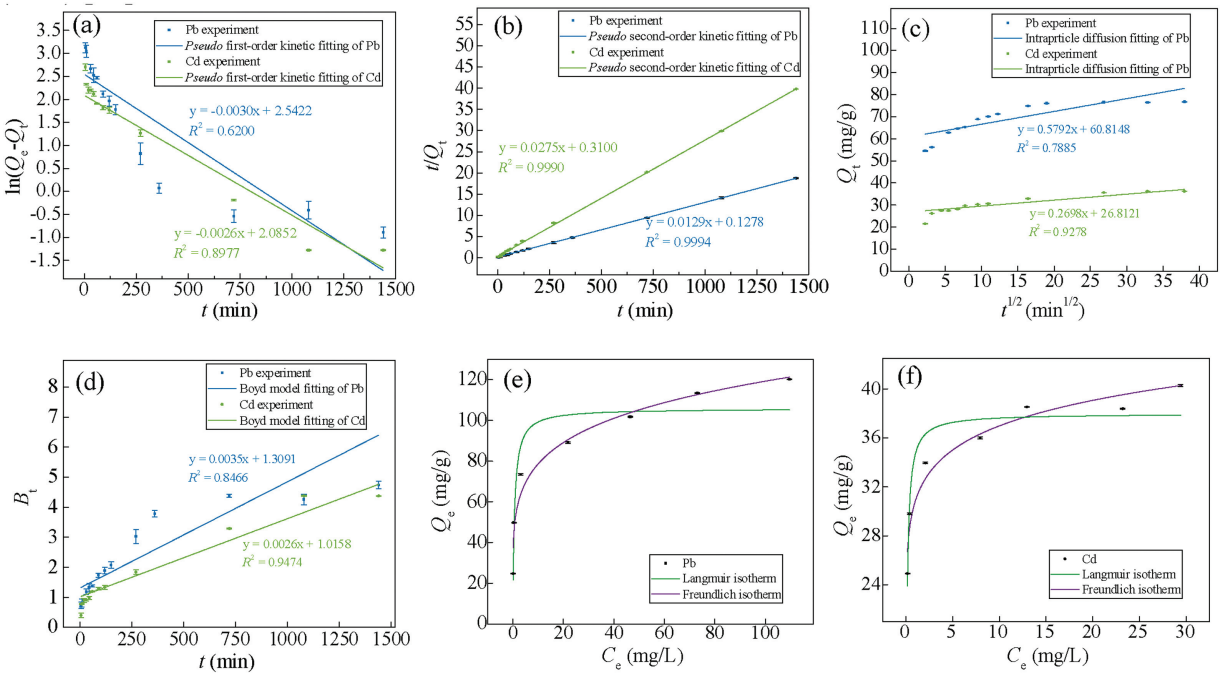

Fig. 4. *Pseudo*-first-order model (a), *pseudo*- second-order model (b), intra-particle diffusion model (c), boyd model (d) for Pb(II) and Cd(II) on Si-Fh. Langmuir isotherm model and Freundlich isotherm model for Pb(II) (e) and Cd(II) (f) adsorption on Si-Fh adsorbents. The error bars represent the standard deviations in triplicate ($n = 3$). Reaction conditions: Si-Fh concentration = 0.2 g/L, Pb concentration = 0.16 g/L, Cd concentration = 0.08 g/L, reaction temperature = 25 °C.

retarded the adsorption rate [39]. As can be seen from Fig. 4d, the straight line of the Boyd model did not pass through the origin thus indicated that the rate was also controlled by membrane diffusion. These two models confirmed that intraparticle diffusion and surface diffusion work together in adsorption process.

The maximum adsorbed capacity is an important evaluation factor for adsorbents. Thus the interaction between Si-Fh and both heavy metals was further studied by adsorption isotherms and the equilibrium data were fitted to the Freundlich and Langmuir isotherms model in Figs. 4e and f. All the sorption parameters were presented in Table S2 (Supporting information).

Two models were used to fit the adsorption isotherms. The equations are as follows:

Langmuir model (Eq. 9):

$$Q_e = \frac{Q_m \cdot K_l \cdot C_e}{1 + C_e} \quad (9)$$

Freundlich model (Eq. 10):

$$Q_e = K_f \cdot C_e^{1/n} \quad (10)$$

where Q_m (mg/g) is the theoretical maximum adsorption capacity, K_l (L/mg) is the Langmuir adsorption equilibrium parameter, and K_f and $1/n$ are the Freundlich adsorption parameters, which reflects the adsorption affinity and heterogeneity of the adsorption sites, respectively.

The Langmuir model argues that the adsorption is a monolayer layer adsorption onto the adsorbent surface homogeneously. The Freundlich isotherm suggests that the surface is heterogeneous therefore the adsorption is multi-layer. Moreover, the adsorption capacity is dependent on the equilibrium concentration of contaminants [40]. It was observed in Figs. 4e and f that with the increase of initial concentration of Pb(II) and Cd(II), the adsorption capacity of Pb(II) and Cd(II) quickly increased until a saturation point was reached and eventually became almost level, which means that the adsorption on Si-Fh surface is saturated. It can be clearly seen that the Freundlich model showed a better match than the Langmuir model for the plots of Q_e. Comparing of nonlinear correlation coefficients R^2 values, it was also found that Freundlich model was more consistent with the adsorption process where samples had higher R^2 (0.9519, 0.9462 for Pb and Cd, respectively). The n values obtained from Freundlich equation were higher than 2, indicating the adsorption process of Pb(II) and Cd(II) by Si-Fh was favorable [40].

It can be concluded from the adsorption kinetics and isotherm experiments results that Si-Fh adsorbed Pb(II) and Cd(II) through chemisorption like most other adsorbents. Mainly functional groups in the adsorption process can be identified through characterization analysis. It can also be concluded from SEM-EDX results that the distribution of Pb(II) and Cd(II) are consistent with O atoms. The FTIR results also demonstrated the adsorption is related to the O through the new bands related to the appearance of O—M bands after adsorption. The XPS results revealed that the contributing specific functional groups are —OH and Si—O bands on the surface of Si—Fh. The hydroxyl groups provided abundant active sites for surface chelation or complexation. In addition, the surface precipitation of metal hydroxides might play a part in the process of removal. We can further confirmed that the inner- and outer- sphere complex was formed and the electrostatic attraction also play a role in the adsorption process from the results of ion strength experiments [41].

An easy coprecipitation method was used for preparing Si—Fh adsorbents to remove Pb(II) and Cd(II) in this paper. The effect of initial pH, ion strength, adsorption kinetics and isotherms were studied. The removal efficiency decreased with the increasing of Na ion concentration. The adsorption behaviors followed the Freundlich model, and the results of maximum adsorption capacity confirmed that Si-Fh exhibited remarkable removal of Pb and Cd. The adsorption of Pb and Cd on Si-Fh was fitted to the *pseudo*-second order kinetics, which means the adsorption process was mainly through chemisorption. The intraparticle diffusion and Boyd model suggest that the intraparticle diffusion and membrane diffusion are both rate limiting steps in the adsorption process. The adsorption was mainly through the complexation of surface functional groups such as Si—O bands and hydroxyl functional groups.

Declaration of competing interest

We have no conflicts of interest to declare.

Acknowledgments

This work was kindly supported by the National Natural Science Foundations of China (Nos. 41771341 and 51978319).

Appendix A. Supplementary data

Supplementary material related to this article can be found, in the online version, at doi:https://doi.org/10.1016/j.cclet.2021.02.062.

References

[1] N. Liu, L. Shi, X. Han, et al., Chin. Chem. Lett. 31 (2020) 386–390.
[2] C. Ling, Y. Zhao, Z. Ren, et al., Chin. Chem. Lett. 30 (2019) 2196–2200.
[3] J. Filip, R. Zboril, O. Schneeweiss, et al., Environ. Sci. Technol. 41 (2007) 4367–4374.
[4] Z. Ding, F. Fu, D.D. Dionysiou, B. Tang, Environ. Pollut. 235 (2018) 660–669.
[5] E. Cabello, Md.P. Morales, C. Serna, et al., Clays Clay Miner. 57 (2009) 46–53.
[6] A.C. Cismasu, F.M. Michel, A.P. Tcaciuc, G.E. Brown, Geochim. Cosmochim. Acta 133 (2014) 168–185.
[7] P. Anderson, M. Benjamin, Environ. Sci. Technol. 19 (1985) 1048–1053.
[8] L. Dyer, P.D. Fawell, O.M.G. Newman, W.R. Richmond, J. Colloid Interface Sci. 348 (2010) 65–70.
[9] R. Vempati, R. Loeppert, Clays Clay Miner. 37 (1989) 273–279.
[10] L. Zhu, F. Fu, B. Tang, Sci. Total Environ. 696 (2019) 133966.
[11] N. Gao, K. Ma, T. Ding, et al., Chin. Chem. Lett. 29 (2018) 482–484.
[12] Z. Lin, X. Weng, G. Owens, Z. Chen, J. Clean. Prod. 242 (2020) 118476.
[13] H. Wang, J. Zhang, P. Wang, et al., Chin. Chem. Lett. 31 (2020) 2789–2794.
[14] K. Menad, A. Feddag, T. Juhna, J. Inorg. Organomet. Polym. Mater. 29 (2019) 1–16.
[15] X. Zhu, W. Jiang, W. Cui, et al., Chin. Chem. Lett. 30 (2019) 1133–1136.
[16] G. Naren, A. Miyazaki, M. Matsuo, et al., Chin. J. Geochem. 32 (2013) 27–34.
[17] L. Carlson, U. Schwertmann, Geochim. Cosmochim. Acta 45 (1981) 421–429.
[18] C. Guo, X. Guo, W. Chu, et al., Chin. Chem. Lett. 31 (2020) 150–154.
[19] R. Vempati, R. Loeppert, D. Dufner, D. Cocke, Soil Sci. Soc. Am. J. 54 (1990) 695–698.
[20] S. Glasauer, J. Friedl, U. Schwertmann, J. Colloid Interface Sci. 216 (1999) 106–115.
[21] S. Glasauer, Lt. Hug, P. Weidler, A. Gehring, Clays Clay Miner. 48 (2000) 51–56.
[22] J. Groenenberg, S. Lofts, Environ. Toxicol. Chem. 33 (2014) 2181–2196.
[23] A.P. Grosvenor, B.A. Kobe, M. Biesinger, N. McIntyre, Surf. Interface Anal. 36 (2004) 1564–1574.
[24] M. Koppelman, J. Dillard, ACS Symp. Ser. 18 (1975) 186–201.
[25] H. Wang, Y.F. Tsang, Y.-n. Wang, et al., Clean. Technol. Environ. Policy 20 (2018) 2169–2179.
[26] S. Bao, W. Yang, Y. Wang, et al., J. Hazard. Mater. 381 (2020) 120914.
[27] P. Qu, Y. Li, H. Huang, et al., Chemosphere 241 (2020) 125004.
[28] C. Xu, S. Shi, X. Wang, et al., J. Hazard. Mater. 381 (2020) 120974.
[29] H. Hu, D. Zhang, H. Liu, et al., Chin. Chem. Lett. 32 (2020) 557–560.
[30] W.S.W. Ngah, S. Fatinathan, J. Environ. Manag. 91 (2010) 958–969.
[31] J. Lützenkirchen, J. Colloid Interface Sci. 195 (1997) 149–155.
[32] D. Zhao, G. Sheng, J. Hu, et al., Chem. Eng. J. 171 (2011) 167–174.
[33] Z. Liu, D. Tian, F. Shen, et al., Chin. Chem. Lett. 30 (2019) 2221–2224.
[34] Z. Li, J. Chen, Y. Ge, Chem. Eng. J. 308 (2017) 809–817.
[35] S. Goldberg, J. Colloid Interface Sci. 285 (2005) 509–517.
[36] M. Mohapatra, K. Rout, B.K. Mohapatra, S. Anand, J. Hazard. Mater. 166 (2009) 1506–1513.
[37] M. Schwaab, E. Steffani, E. Barbosa-Coutinho, J.B. Severo Júnior, Chem. Eng. Sci. 173 (2017) 179–186.
[38] C. Zhang, Z. Yu, G. Zeng, et al., Chem. Eng. J. 284 (2015) 247–259.
[39] P.S. Kumar, S. Ramalingam, S.D. Kirupha, et al., Chem. Eng. J. 167 (2011) 122–131.
[40] S. Xin, Z. Zeng, X. Zhou, et al., J. Hazard. Mater. 324 (2017) 365–372.
[41] W. Qiao, P. Zhang, L. Sun, et al., Chin. Chem. Lett. 31 (2020) 2742–2746.